



Phase-based constitutive modeling and experimental study for dynamic mechanical behavior of martensitic stainless steel under high strain rate in a thermal cycle

Zhenguo Nie ^{a,b}, Gang Wang ^{a,b,*}, Jianchao Yu ^{a,b}, Dehao Liu ^{a,b}, Yiming (Kevin) Rong ^{a,b,c}

^a State Key Laboratory of Tribology & Institute of Manufacturing Engineering, Department of Mechanical Engineering, Tsinghua University, Beijing, 100084, China

^b Beijing Key Lab of Precision/Ultra-precision Manufacturing Equipments and Control, Tsinghua University, Beijing, 100084, China

^c Department of Mechanical and Energy Engineering, South University of Science and Technology of China, Shenzhen, 518055, China



ARTICLE INFO

Article history:

Received 2 April 2016

Revised 1 August 2016

Available online 8 August 2016

Keywords:

Phase-based model

Dynamic mechanical behavior

Flow stress loop

Martensitic stainless steel

Creep-feed grinding

ABSTRACT

The material of turbine blades undergoes a complete thermal cycle in creep-feed grinding. The flow stress in the cycle has a significant effect on the residual stress, microtopography, and surface integrity. This study presents a phase-based constitutive model for describing the dynamic mechanical behavior of martensitic stainless steel in a complete thermal cycle. The complete tests were conducted by using thermal compressive deformation via Split Hopkinson Pressure Bar and Gleeble 3500, with temperature ranging from 20 °C to 1000 °C, and strain rate ranging from 0.001 s⁻¹ to 16,000 s⁻¹. Phase transformation kinetics was involved for the dual-phase region, and a modified Johnson-Cook model was employed to determine the dynamic mechanical behavior of single phase. The prediction of the phase-based model correlates well with the experimental data on stress-strain curves. The flow stress is demonstrated to form a loop in a complete thermal cycle, and the results indicated that the temperature history must be considered in the evolution of flow stress in terms of strain, strain rate, and temperature.

© 2016 Elsevier Ltd. All rights reserved.

1. Introduction

Creep-feed grinding is widely used in the manufacturing of turbine blades. Low feed speed and large cutting depth are the two main features in creep-feed grinding. The feed speed is typically below 60 mm/min, and the cutting depth can reach approximately 10 mm (Grigoriev et al., 2014). In association with the high temperature (above 800 °C) (Lefebvre et al., 2012; Yao et al., 2014; Zahedi and Akbari, 2011) and large strain rate ($10^5 \sim 10^6 \text{ s}^{-1}$) (Klocke et al., 2002), the material flowing behavior in the grinding area is a key factor in the material removal mechanism, residual stress formation, microtopography, and product service performance. The single abrasive-grain cutting process was studied to understand the macro-scale grinding process via experiments and simulations (Anderson et al., 2012; Öpöz and Chen, 2012). A constitutive model that is valid over a wide range of temperature and strain rate is essential for predicting the stress field for numerical simulation of creep-feed grinding process.

The workpiece temperature field in creep-feed grinding without coolant was measured via using an infrared thermometer, as shown in Fig. 1. In this case, the linear wheel speed is 20 m/s, the workpiece feed speed is 10 mm/s, and the cutting depth is 100 μm. The maximum temperature reaches about 965 °C, which exceeds the phase transformation point. The phase transformation must be considered in modeling the dynamic mechanical behavior of the material.

When the steel is at an elevated temperature, the flow stress cannot be accurately predicted by the original Johnson-Cook (JC) model (Akbari et al., 2015; Li et al., 2013). The flow stress decreases rapidly around the austenitizing temperature for austenitic stainless steel (Gupta et al., 2013). Many modified models based on mathematical modification have been proposed to solve the problem. Martensitic transformation occurs when the austenite is cooled down below the martensite starting point (M_s). A constitutive model involving phase transformation kinetics was proposed to predict the dynamic mechanical behavior of martensitic transformation at high strain rate (Zaera et al., 2012).

This work presents a phase-based constitutive model of martensitic stainless steel under elevated temperatures in a complete thermal cycle (heating and cooling). The constitutive model contains four stages: the initial microstructure (tempered

* Corresponding author. Fax: +8601062794751.

E-mail addresses: niezhenguo@126.com (Z. Nie), [\(G. Wang\)](mailto:gwang@tsinghua.edu.cn).

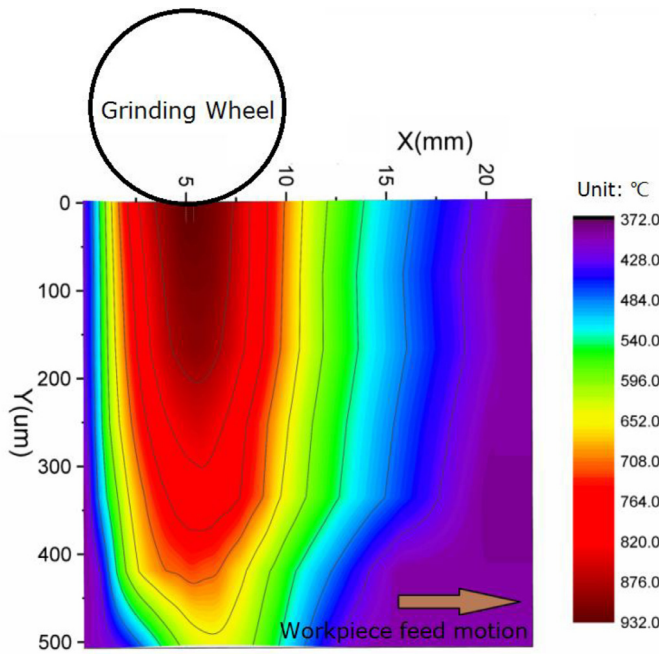


Fig. 1. Temperature field measured via infrared thermometer during creep-feed grinding. (Workpiece material: 2Cr12Ni4Mo3VNbN steel).

Table 1

Chemical composition of 2Cr12Ni4Mo3VNbN steel. (wt. %).

C	Cr	Ni	Mo	Nb	V	N	Fe
0.02%	12.09%	3.46%	3.80%	0.38%	0.47%	1.43%	Balance

martensite) during heating process, the austenitizing process, the austenite during cooling process and the martensitic transformation. The dynamic mechanical behavior of single phases, such as tempered martensite and austenite, was described by using a modified JC model. The phase transformation kinetics was involved in dual-phase regions, i.e., austenitizing and martensitic transformation.

2. Phase-based constitutive model

During a complete thermal cycle, the austenitizing and martensitic transformation occurs in martensitic stainless steel. A phase-based constitutive model was proposed to describe the dynamic mechanical behavior during each transformation stage. A modified JC model was employed for the single phases, at both high and low strain rates.

2.1. Material characteristics of the phase transformation

2Cr12Ni4Mo3VNbN steel is a martensitic stainless steel that is widely used in steam turbine blades due to its excellent corrosion resistance. The chemical composition of 2Cr12Ni4Mo3VNbN steel is listed in [Table 1](#). Chromium and nickel can improve the corrosion resistance in an oxidizing medium. Molybdenum can improve the corrosion resistance in non-oxidizing acid and alkaline solutions. Titanium and niobium form stable carbides with carbon poor chrome.

The thermal dilatometric curve of 2Cr12Ni4Mo3VNbN steel within a thermal cycle is shown in [Fig. 2](#). The austenitizing occurs in the heating process when the temperature reaches the range of A_1 to A_3 . A_1 (698°C) is the starting temperature, and A_3 (886°C) is the final temperature.

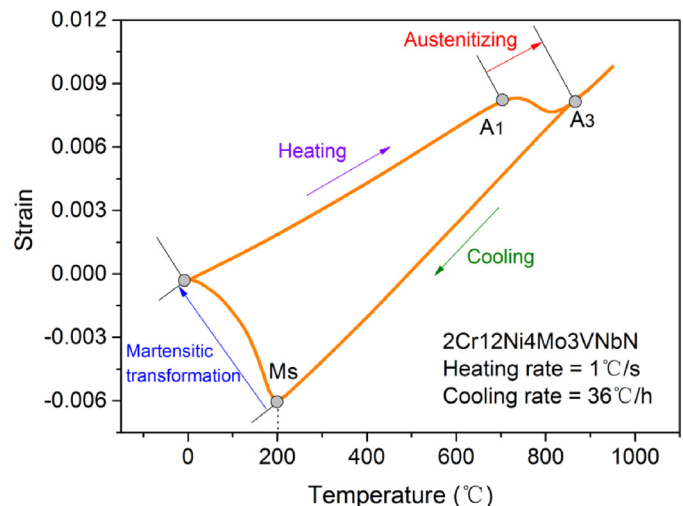


Fig. 2. Thermal dilatometric curve of 2Cr12Ni4Mo3VNbN steel. $A_1 = 698^{\circ}\text{C}$, $A_3 = 886^{\circ}\text{C}$, $M_s = 200^{\circ}\text{C}$. Heating rate = $1^{\circ}\text{C}/\text{s}$ and cooling rate = $36^{\circ}\text{C}/\text{h}$.

The undercooled austenite of 2Cr12Ni4Mo3VNbN steel is quite stable and the critical quenching rate is extremely small. In this experiment, the cooling rate is $36^{\circ}\text{C}/\text{h}$ and only martensitic transformation occurs. In the cooling process, the austenite remains unchanged when the temperature is above M_s (200°C).

2.2. Phase-based constitutive model

The proposed phase-based constitutive model is given by [Eq. \(1\)](#). The flow stress is the weighted algebraic sum of each single phase, and the weight factor is the volume fraction of the single phase.

$$\sigma = \sum_i \xi_i \cdot \sigma_i = \sum_i f_i(T, \sigma, \varepsilon) \cdot \sigma_i(T, \varepsilon, \dot{\varepsilon}) \quad (1)$$

where σ is the flow stress, ξ_i is the volume fraction of single phase i , and σ_i is the partial stress of phase i . $\xi_i = f_i(T, \sigma, \varepsilon)$ is a function

of the temperature T , flow stress σ and strain $\sigma_i = \sigma_i(T, \varepsilon, \dot{\varepsilon})$ is the constitutive equation of single phase i .

In 2Cr12Ni4Mo3VNBN steel, the phase-based constitutive model can be interpreted as involving four stages: heating, austenitizing process, cooling, and martensitic transformation.

$$\sigma = \begin{cases} \sigma_{tm}, & \text{in heating} \\ (1 - \xi_y)\sigma_{tm} + \xi_y\sigma_y, & \text{in austenitizing process} \\ \sigma_y, & \text{in cooling} \\ (1 - \xi_m)\sigma_y + \xi_m\sigma_m, & \text{in martensitic transformation} \end{cases} \quad (2)$$

where σ_{tm} is the flow stress of tempered martensite, σ_y is the flow stress of austenite, σ_m is the flow stress of martensite, ξ_y is the volume fraction of austenite during austenitizing, and ξ_m is the volume fraction of martensite during martensitic transformation.

2.3. Modified JC model of single phase at both high and low strain rates

As shown in Eq. (3), a modified JC model was proposed to describe the dynamic mechanical behavior for a single phase. The modified model can predict the dynamic mechanical behavior of single phase better than the original JC model at both high and low strain rates. The fitting results will be provided in the following section.

$$\sigma_i(T, \varepsilon, \dot{\varepsilon}) = (A + B\varepsilon_e^n)(1 + C(\ln \dot{\varepsilon}_e^*)^p)(1 - (T^*)^m) \quad (3)$$

$$\dot{\varepsilon}_e^* = \frac{\dot{\varepsilon}}{\dot{\varepsilon}_0} \quad (4)$$

$$T^* = \frac{T - T_r}{T_m - T_r} \quad (5)$$

where A , B , n , C , p , and m are material constants, A is the yield strength (MPa), B is the hardening modulus (MPa), n is the hardening coefficient, C and p are the strain rate sensitivity coefficients, and m is the thermal softening coefficient. $\dot{\varepsilon}_e^*$ is a dimensionless parameter, $\dot{\varepsilon}$ is the strain rate, and $\dot{\varepsilon}_0$ is the reference strain rate. T_r is the reference temperature and T_m is the melting temperature of the material.

3. Experimental design

Dynamic mechanical behavior tests were conducted on SHPB and Gleeble 3500. The strain rate ranges from 10^{-3} s^{-1} to 10^5 s^{-1} , and the temperature ranges from 20°C to 1000°C .

3.1. Experimental schematics

In a complete thermal cycle, the material experiences four stages: heating, austenitizing process, cooling, and martensitic transformation. There are three single phases in 2Cr12Ni4Mo3VNBN steel: the initial microstructure (tempered martensite), austenite, and martensite. There are two phase transformation regions: austenitizing process and martensitic transformation.

The experimental schematics are presented in Fig. 3. For the heating stage, the specimen was heated to the target temperature T_1 , and then deformed at a certain strain rate $\dot{\varepsilon}$. For the cooling stage, the specimen was heated to 900°C , and then insulated for 10 min for complete austenitizing. Next the specimen was cooled down to the target temperature T_2 , and then deformed at a certain strain rate $\dot{\varepsilon}$. All the parameters are listed in Table 2.

Cylindrical specimens were used in this experiment. The dimensions of the specimen were $\varnothing 2(\text{mm}) \times 2(\text{mm})$ in the high strain rate tests, and $\varnothing 8(\text{mm}) \times 10(\text{mm})$ in the quasi-static tests ($\dot{\varepsilon} = 0.001 \text{ s}^{-1}$). All the specimens were oil-quenched and tempered before testing. The tempering temperature was 610°C , and the holding time was 3 h. As shown in Fig. 4, the initial microstructure was tempered martensite.

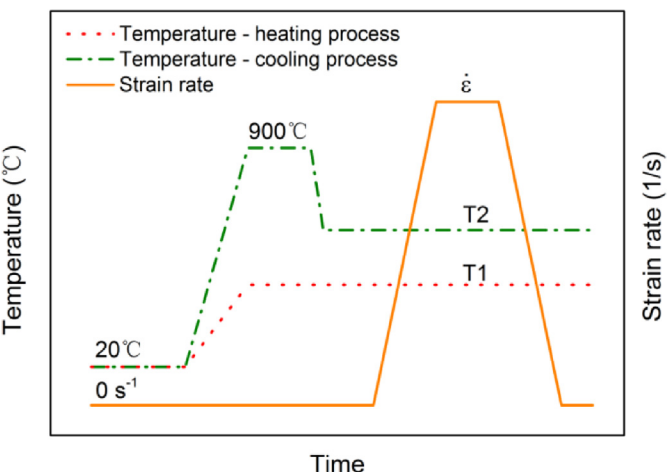


Fig. 3. Schematics of dynamic mechanical behavior test.

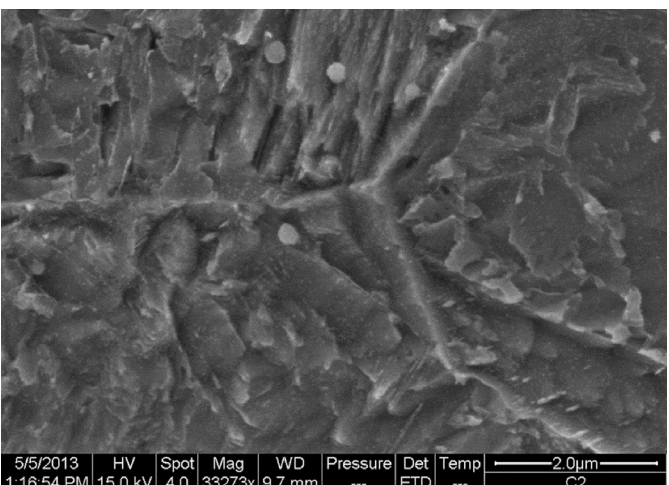


Fig. 4. SEM micrograph of tempered martensite in 2Cr12Ni4Mo3VNBN steel.

3.2. High strain rate tests

The SHPB apparatus was used for the dynamic mechanical behavior tests at high strain rate. Fig. 5 shows the schematics of the SHPB system. The system contains two long elastic bars: the incident bar and the transmitted bar. A small cylindrical specimen is placed between the two bars. The impact of the strike to the incident bar generates a stress pulse. The stress pulse travels in the incident bar, and then some energy is reflected at the interface of the incident bar and specimen (surface 1). The remaining energy is transmitted to the transmitted bar. The elastic strains of the two bars are recorded by the strain gages. The stress, strain, and strain rate of the specimen can be calculated based on the theory of one dimensional wave propagation (Lindholm, 1964). The two bars and strike are all made of ultra-high strength steel with the yield strength of around 2000 MPa.

The strike was driven by high-pressure nitrogen to a certain speed, and then impacted onto the incident bar. As shown in Fig. 6, the incident strain signal is ε_i , the reflected strain signal is ε_r , and the transmitted strain signal is ε_t . The relationship among the three strain signals is shown in Eq. (6).

$$\varepsilon_i(t) + \varepsilon_r(t) = \varepsilon_t(t) \quad (6)$$

Table 2
Experimental parameters.

Stage	Temperature (T)/°C	Strain rate ($\dot{\varepsilon}$)/s ⁻¹
Heating	20, 200, 400, 500, 600, 700, 775*, 800*	0.001, 1100, 2400, 4000, 8000, 16,000
Cooling	1000, 800, 600, 400, 200, 100*, 20	0.001, 1000, 3000, 10,000, 16,000

* The asterisk indicates that phase transformation occurs at the current temperature.

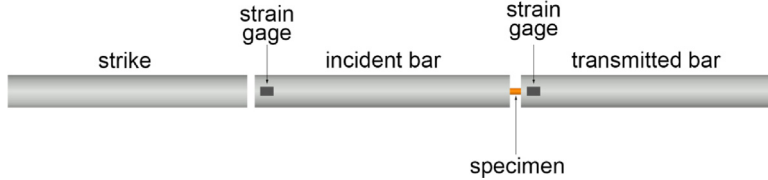


Fig. 5. Schematics of the SHPB system.

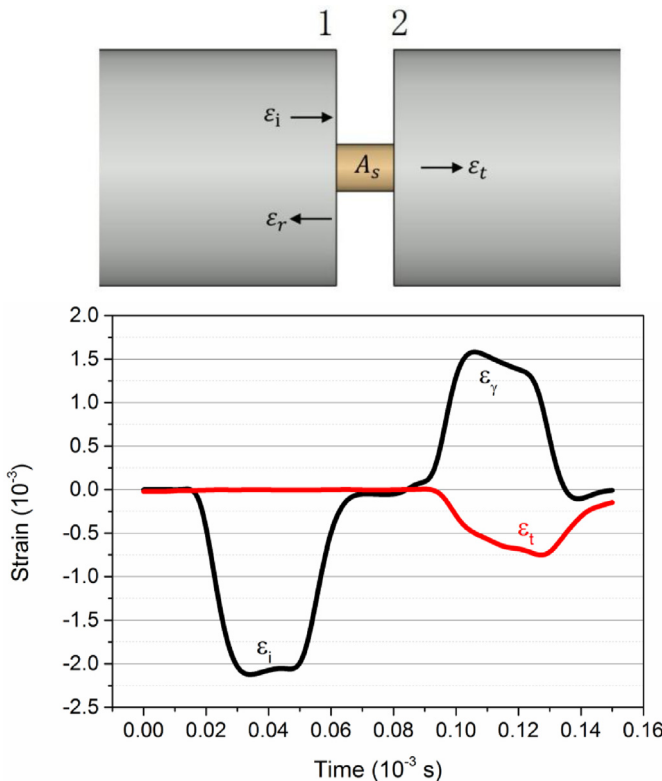


Fig. 6. Elastic strain signal waves during impact process.

The displacements of surface 1 and surface 2 in Fig. 6 can be calculated by Eqs. (7) and (8).

$$u_1 = C_0 \int_0^t (\varepsilon_i - \varepsilon_r) dt \quad (7)$$

$$u_2 = C_0 \int_0^t \varepsilon_t dt \quad (8)$$

where u_1 is the displacement of surface 1, u_2 is the displacement of surface 2, C_0 is the elastic wave speed within the bars.

Then the engineering strain ε_e of the specimen can be calculated as Eq. (9).

$$\varepsilon_e = \frac{u_1 - u_2}{L} = \frac{C_0}{L} \int_0^t (\varepsilon_i - \varepsilon_r - \varepsilon_t) dt \quad (9)$$

From Eqs. (6) and (9), the engineering strain ε_e of the specimen can be finally expressed as Eq. (10). Taking the derivative of the

engineering strain ε_e , strain rate $\dot{\varepsilon}$ can be obtained in Eq. (11).

$$\varepsilon_e = -\frac{2C_0}{L} \int_0^t \varepsilon_r dt \quad (10)$$

$$\dot{\varepsilon} = \frac{d\varepsilon_e}{dt} = -\frac{2C_0}{L} \varepsilon_r \quad (11)$$

According to Newton's Third Law of Motion, the action forces applied on surface 1 and surface 2 of specimen are equal to the reaction forces applied on surface 1 and surface 2 of bars. The two action forces applied on surface 1 and surface 2 can be determined by Hooke's Law as presented in Eq. (12).

$$\begin{cases} F_1 = EA(\varepsilon_i + \varepsilon_r) \\ F_2 = EA\varepsilon_t \end{cases} \quad (12)$$

where F_1 is the action force applied on surface 1, F_2 is the action force applied on surface 2, E is the Young's modulus of bars, A is the cross section area of bars.

The average engineering stress of specimen can be expressed as:

$$\sigma_e = \frac{F_1 + F_2}{2A_s} = \frac{1}{2} E \left(\frac{A}{A_s} \right) (\varepsilon_i + \varepsilon_r + \varepsilon_t) = E \left(\frac{A}{A_s} \right) \varepsilon_t \quad (13)$$

where A_s is the cross section area of specimen.

True strain ε_s and true stress σ_s can be transformed from engineering strain ε_e and engineering stress σ_e by Eqs. (14) and (15).

$$\varepsilon_s = -\ln(1 - \sigma_e) \quad (14)$$

$$\sigma_s = \sigma_e(1 - \varepsilon_e) \quad (15)$$

From Eqs. (10), (13), (14), and (15), the relationship between true stress and true strain can be derived by eliminating the time items.

As shown in Figs. 7 and 8, the SHPB system used in the experiment allows the strain rates to vary from 10^3 s⁻¹ to 10^5 s⁻¹, including the whole temperatures in Table 2. The specimen was fixed into the furnace by a metal wire during heating process before impact. The incident and transmitted bars were both out of the furnace to avoid being heated. Temperature was measured by thermocouple wires which welded on the specimen. When the temperature of the specimen reached a target point, two bars would be moved fast into the furnace to clamp the specimen manually, and then the impact was started.

The SHPB test is an adiabatic process, so the increase in temperature during the plastic deformation cannot be ignored. The temperature rise can be calculated by Eq. (16). The temperature rise caused by adiabatic process will be taken into account in drawing the stress-strain curves.

$$\Delta T = \int_0^\varepsilon \frac{\sigma}{\rho C_V} d\varepsilon \quad (16)$$



Fig. 7. High strain rate tests on the SHPB system.

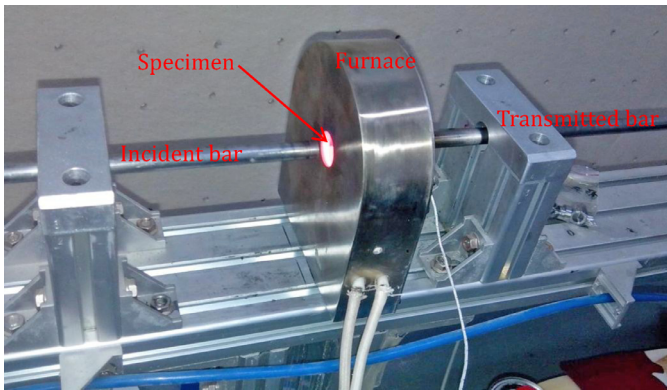


Fig. 8. Specimen was heated in the furnace before impact.



Fig. 9. Quasi-static compression tests on the Gleeble 3500 thermal simulator.

where ρ is density, and C_V is heat capacity at a constant volume.

3.3. Quasi-static tests

For the quasi-static tests, Gleeble 3500 thermal simulator was used to compress the specimens at the strain rate of 10^{-3} s^{-1} . As shown in Fig. 9, Gleeble 3500 is a fully integrated digital closed loop control thermal and mechanical test system. The stress-strain curves were obtained after the compressive tests.

4. Modified JC model for single phase

The modified JC model is proposed for both tempered martensite and austenite. All the parameters of the modified JC model can be fitted based on the experimental data. It turns out that the modified JC model can well predict the dynamic mechanical behavior of each single phase, under both low and high strain rates.

4.1. Dynamic mechanical behavior of tempered martensite and martensite

Fig. 10 shows the dynamic mechanical behavior of tempered martensite and martensite. It is obvious that the flow stress increases with the increasing plastic strain and strain rate, but decreases with the increasing temperature. As the two phases have almost the same mechanical behavior, the same modified JC model was adopted for both the tempered martensite and the martensite.

The modified JC model in Eq. (3) has three parts: $(A + B\varepsilon_e^n)$ is strain hardening item, $(1 + C(\ln\dot{\varepsilon}_e)^p)$ is strain rate hardening item, and $(1 - (T^*)^m)$ is thermal softening item. All the unknown parameters can be fitted in three steps (Hou and Wang, 2010): (a) The strain-hardening item can be fitted by using stress-strain curve under quasi-static state and room temperature. (b) The strain rate hardening item can be fitted by using stress-strain curves with various strain rates under room temperature. (c) The thermal softening item can be fitted by comparing the stresses under various temperatures.

Based on the experimental data in Fig. 10, all the parameters of the modified JC model presented in Eq. (3) are fitted as follows:

$$A = 1107.90 \text{ MPa}, B = 444.56 \text{ MPa}, n = 1.17 \times 10^{-1}, C = 3.10, \dot{\varepsilon}_0 = 0.001 \text{ s}^{-1}, p = 4.86, m = 1.05, T_r = 20^\circ\text{C}, T_m = 1433^\circ\text{C}$$

The experimental data and fitting curves of tempered martensite (and martensite) are also compared in Fig. 10. The comparison results indicate that the modified JC model can accurately describe the dynamic mechanical behavior of tempered martensite (and martensite).

4.2. Dynamic mechanical behavior of austenite

There is no diffusive transformation in 2Cr12Ni4Mo3VNbN steel. The austenite remains stable when the temperature is below than A_3 . The martensitic transformation occurs only when the temperature is below than M_s .

The dynamic mechanical behavior of austenite is presented in Fig. 11. Similar in many aspects to tempered martensite, the flow stress increases with the increasing plastic strain and strain rate, but decreases with the increasing temperature. The modified JC model is similarly used to describe the mechanical behavior of austenite in Eq. (3). All of the parameters are fitted as follows:

$$A = 377.63 \text{ MPa}, B = 699.57 \text{ MPa}, n = 3.97 \times 10^{-1}, C = 2.95, \dot{\varepsilon}_0 = 0.001 \text{ s}^{-1}, p = 4.12, m = 1.49, T_r = 200^\circ\text{C}, T_m = 1433^\circ\text{C}$$

The experimental data and fitting results are also compared in Fig. 11. The prediction of the modified JC model corresponds well with experimental results from low (0.001 s^{-1}) to high ($16,000 \text{ s}^{-1}$) strain rates for austenite at elevated temperatures.

5. Phase-based model for dual-phase region

The austenitizing process and martensitic transformations occur in two-phase regions. The content of phases varying with temperature has a significant influence on the mechanical properties. The volume fraction of the phases must be distinguished and weighted in the constitutive models.

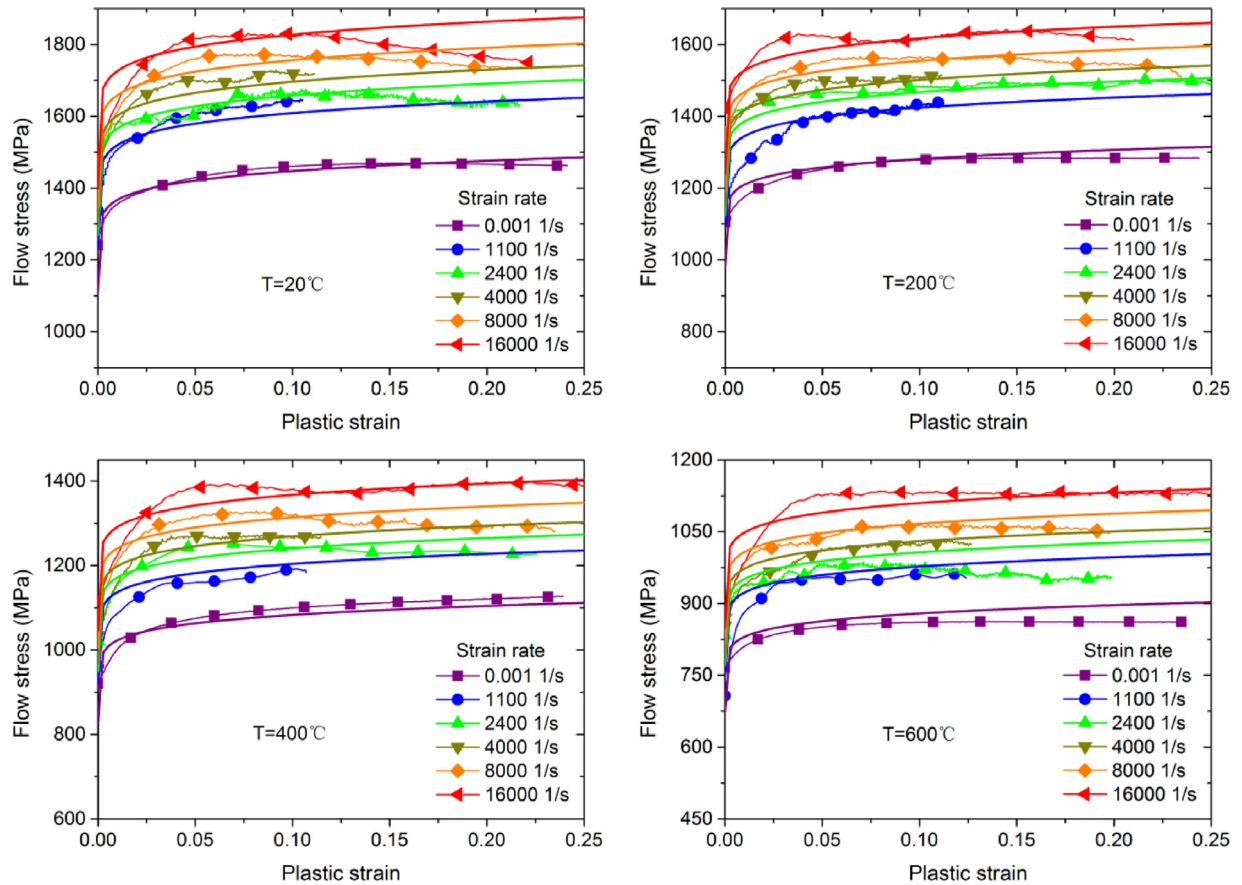


Fig. 10. Comparison of experimental stress-strain curves and fitting results of tempered martensite and martensite.

5.1. Dynamic mechanical behavior in the austenitizing process

During the austenitizing process, the initial microstructure transforms into austenite. The phase transformation kinetics of austenitizing was determined. Next, the phase-based constitutive model of the material in austenitizing process was constructed; the model accurately fits the experimental data.

5.1.1. Phase transformation kinetics of austenitizing process

The volume rate of austenite during austenitizing can be quantified by using dilatometric analysis (Pacyna, 2011; Suh et al., 2007) as shown in Fig. 12. The solid line is the dilatometric strain curve. Point A_1 is the starting point of austenitizing, and point A_3 is the ending point. Suppose that point P is located on the dilation-temperature curve corresponding to a certain temperature T . The vertical line MN passing through point P intersects two extended lines at M and N. Thus, the volume fraction of austenite is expressed as:

$$\xi_\gamma(T) = \frac{|\text{MP}|}{|\text{MN}|} \quad (17)$$

For an isothermal solid state phase transformation, Johnson-Mehl-Avrami (JMA) equation is used to describe the transformation kinetics, as shown in Eqs. (18) and (19) (Callister and Rethwisch, 2007).

$$\xi_\gamma = 1 - \exp(-\beta^n) \quad (18)$$

$$\beta = k_0 \cdot \exp\left(-\frac{Q}{RT}\right) \cdot t \quad (19)$$

When the austenitizing process is non-isothermal, for example, the continuous heating, β in Eq. (19) can be calculated by integral

form or by dispersion sum as follows (Zhang et al., 2002):

$$\beta = \int_0^t k_0 \cdot \exp\left(-\frac{Q}{RT}\right) \cdot dt \quad (20)$$

$$\beta = \sum_{i=1}^m \Delta t \cdot k_0 \cdot \exp\left(-\frac{Q}{RT_i}\right) \quad (21)$$

The activation energy Q is calculated by using Kissinger method as follows (Kissinger, 1957):

$$\ln \frac{\dot{T}}{T_m^2} = -\frac{Q}{RT_m} + C \quad (22)$$

where \dot{T} is heating rate, and T_m is the temperature at which the peak differential thermal analysis deflection occurs, as shown in Fig. 13.

The parameter n and k_0 can be calculated by Eq. (23).

$$\frac{\beta}{k_0} = \frac{\Delta T}{\dot{T}} \sum_{i=1}^m \exp\left(-\frac{Q}{RT_i}\right) \quad (23)$$

All of the parameters in Eqs. (18) and (20) are fitted as follows: $Q = 2.476 \times 10^6 \text{ J/mol}$, $n = 0.3406$, $\ln k_0 = 110.7$ (Nie et al., 2014).

5.1.2. Constitutive model of austenitizing process

The phase-based constitutive model of dual-phase region during the austenitizing process can be presented as follows:

$$\sigma = (1 - \xi_\gamma) \cdot \sigma_{tm}(T, \varepsilon, \dot{\varepsilon}) + \xi_\gamma \cdot \sigma_\gamma(T, \varepsilon, \dot{\varepsilon}) \quad (24)$$

where $\sigma_{tm}(T, \varepsilon, \dot{\varepsilon})$ is the flow stress of tempered martensite, and $\sigma_\gamma(T, \varepsilon, \dot{\varepsilon})$ is the flow stress of austenite. ξ_γ is the volume fraction of austenite at temperature T calculated by Eq. (17). It can be seen

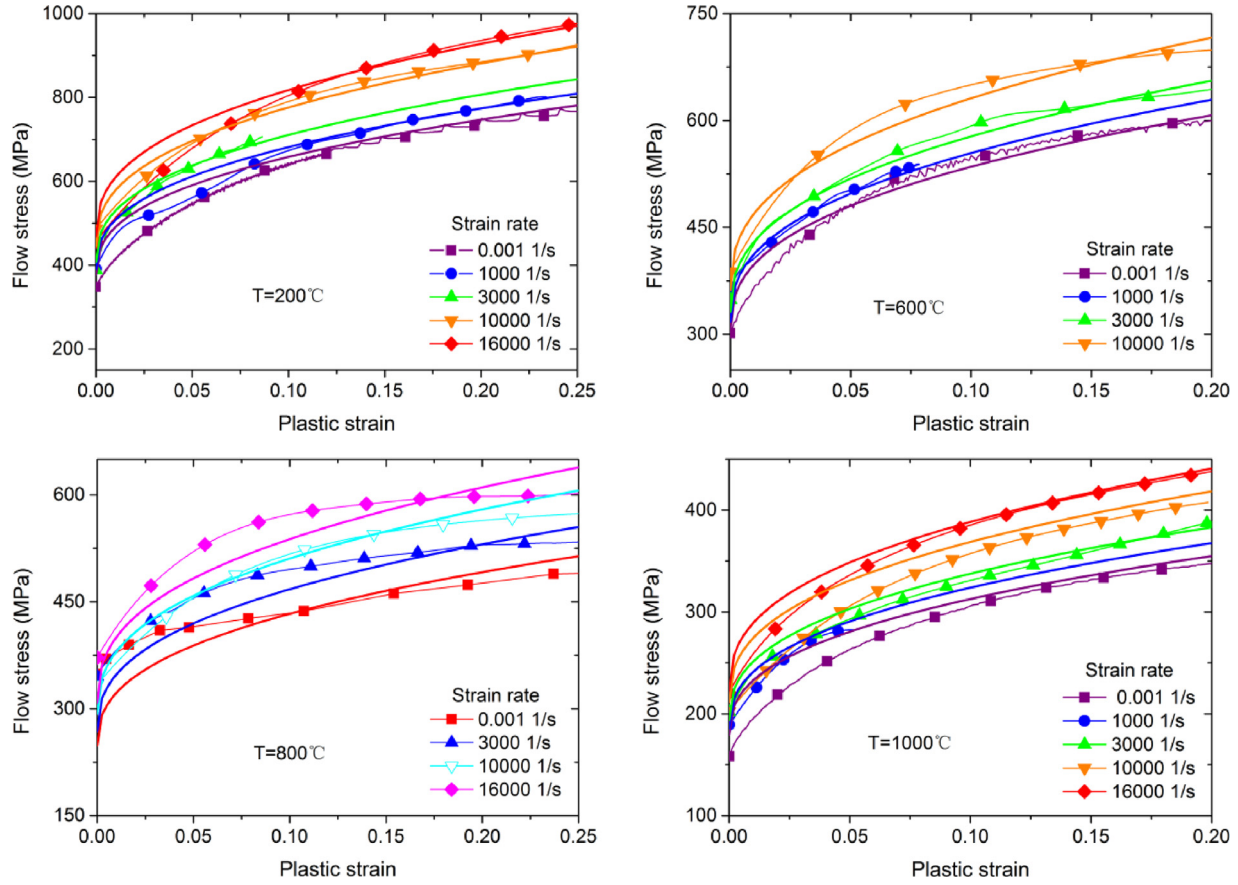


Fig. 11. Comparison of experimental stress-strain curves and fitting results of austenite.

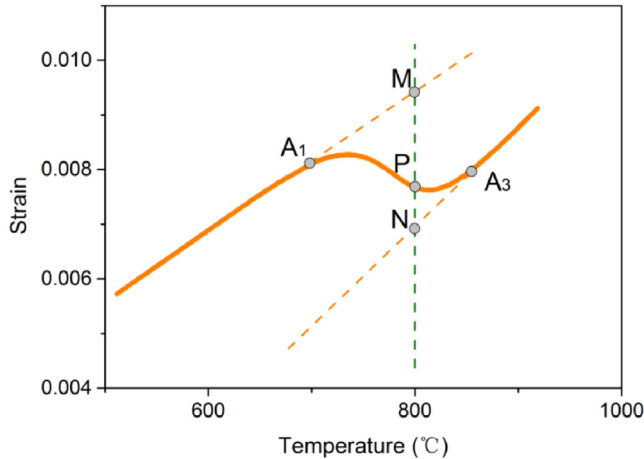


Fig. 12. Dilatometric curve of 2Cr12Ni4Mo3VNbN steel during austenitizing process.

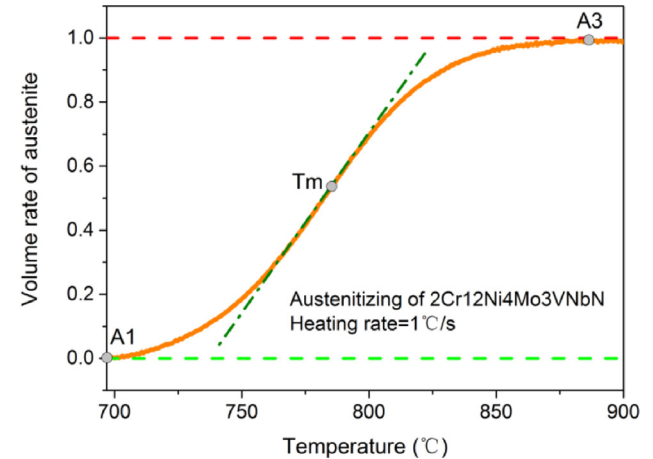


Fig. 13. Volume rate of austenite during austenitizing process in 2Cr12Ni4Mo3VNbN steel.

in Fig. 12 that the volume fraction of austenite is approximately 46% at 775 °C, and 71% at 800 °C.

As shown in Fig. 14, the blue curve is $\sigma_{tm}(T, \varepsilon, \dot{\varepsilon})$, and the red one is $\sigma_y(T, \varepsilon, \dot{\varepsilon})$. The green curve is $(1 - \xi_y) \cdot \sigma_{tm}(T, \varepsilon, \dot{\varepsilon}) + \xi_y \cdot \sigma_y(T, \varepsilon, \dot{\varepsilon})$ which accounts for two phases. The phase-based predicted value is in good agreement with the experimental data. Neither the blue curve nor the red curve can describe the experimental data as phase transformation. It is unreasonable to predict the constitutive relationship by a single constitutive equation in the two-phase region.

5.2. Dynamic mechanical behavior during martensitic transformation

When the austenite is cooled down to M_s , austenite starts to transform into martensite. The KM equation is used to describe the kinetics of the martensitic transformation, and then involved in the phase-based constitutive model during martensitic transformation. The comparison result shows that the phase-based model fits the experimental data well.

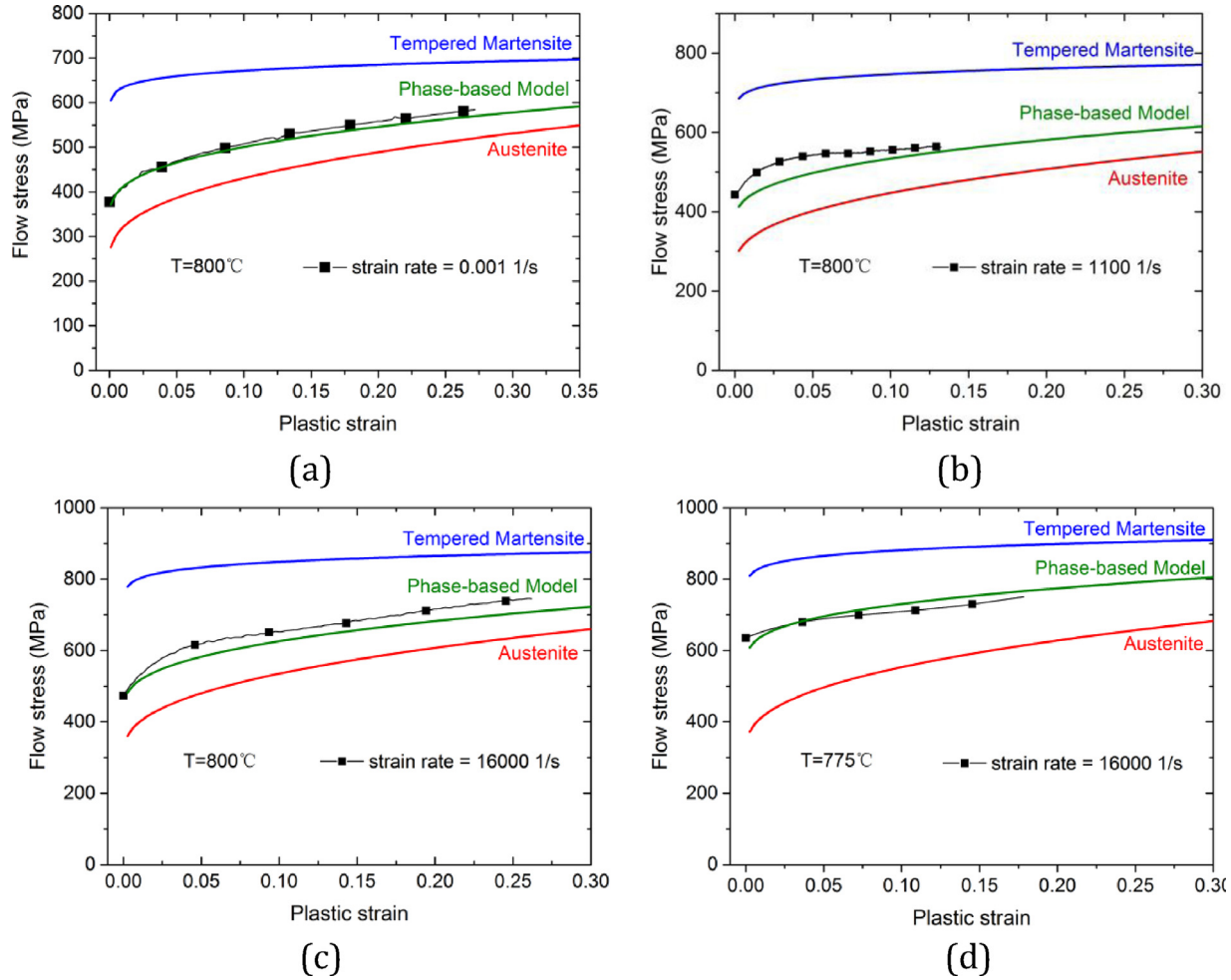


Fig. 14. Comparison of stress-strain curves and fitting results during austenizing process.

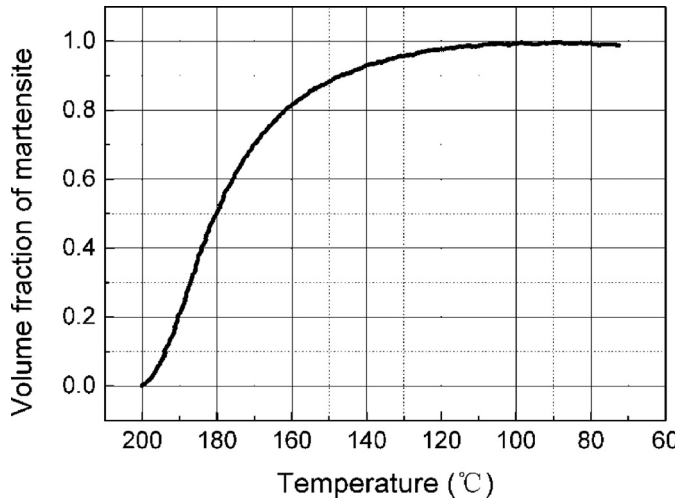


Fig. 15. The volume fraction of martensite during martensitic transformation.

5.2.1. Kinetics of the martensitic transformation

The volume fraction of martensite during martensitic transformation can be determined by using dilatometric analysis. The volume fraction of martensite can be obtained by lever rule as shown in Fig. 15.

As expressed in Eq. (25), the KM equation is used to predict the kinetics of martensitic transformation (Koistinen and Marburger, 1959).

$$\xi_m(T) = 1 - \exp[\alpha(M_s - T)] \quad (25)$$

Based on the experimental data in Fig. 15, the unknown parameters in Eq. (25) can be fitted as follows: $\alpha = -0.03275$, $M_s = 200$ °C. It can be seen that ξ_m is 0.71 when the temperature is 100 °C during the martensitic transformation.

5.2.2. Constitutive model of the martensitic transformation

During the martensitic transformation, the microstructure consists of austenite and martensite. The phase-based constitutive model of the two-phase region during the martensitic transformation can be represented as follows:

$$\sigma = \xi_m \cdot \sigma_m(T, \varepsilon, \dot{\varepsilon}) + (1 - \xi_m) \cdot \sigma_\gamma(T, \varepsilon, \dot{\varepsilon}) \quad (26)$$

where $\sigma_m(T, \varepsilon, \dot{\varepsilon})$ is the flow stress of martensite, and $\sigma_\gamma(T, \varepsilon, \dot{\varepsilon})$ is the flow stress of austenite. ξ_m is the volume fraction of martensite at temperature T which is below M_s .

The phase-based constitutive model of martensitic transformation can be verified by experimental results as shown in Fig. 16. When the austenite is cooled down to 100 °C, approximately 71% of the austenite changes into martensite. The blue curve is the stress-strain of martensite at 100 °C, and the red one is the extrapolated stress-strain curve of austenite at 100 °C. The green curve is the stress-strain of the two-phase mixture calculated by Eq. (26) in

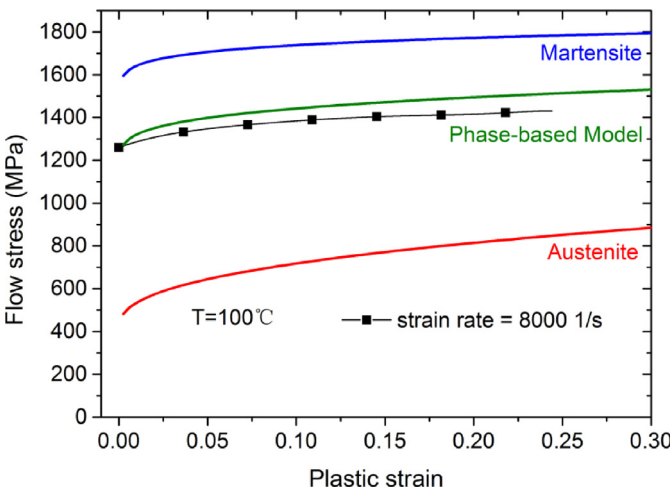


Fig. 16. Comparison of stress-strain curves and fitting results during martensitic transformation.

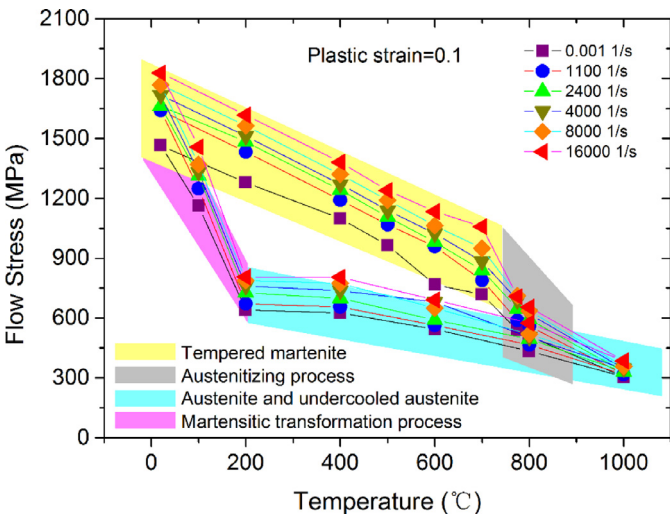


Fig. 17. Variations of the flow stress with temperature in a complete thermal cycle form a flow stress loop. The plastic strain is 0.1.

which $\xi_M = 0.71$. It is observed that the calculated curve fits the experimental data well.

6. Discussion

6.1. Flow stress loop in a complete thermal cycle

As shown in Fig. 17, the variations of flow stress with temperature form a flow stress loop (FSL) in a complete thermal cycle under different strain rates. The yellow block is initial microstructure (tempered martensite). The flow stress decreases with the increases in temperature, this behavior is called thermal softening effect. The grey block is austenizing process, and the flow stress decreases rapidly during phase transformation. The cyan block is austenite, and the pink block is martensitic transformation. Martensite has high hardness and high strength, nearly the same as those of the tempered martensite. The four blocks form a closed flow stress loop. The yellow and cyan are single-phase blocks, and the other two are dual-phase blocks.

Flow stress is not a single-valued function at a certain temperature. The stress-strain behavior depends on not only the temperature, but also the temperature history. This temperature-history

dependence is the significant difference between the phase-based model and other constitutive models.

6.2. Strain rate sensitivity in bcc and fcc crystal structures

Martensite and tempered martensite are body-centered cubic (bcc) metal. In bcc metals, the thermal yield stress is strongly dependent on the strain rate and temperature. Such behavior is considered to indicate the Peierls–Nabarro stress (short-range barriers) being overcome through a ledge wise motion of dislocation kinks. Austenite is face-centered cubic (fcc) metal. In the case of fcc metals, the rate-controlling mechanism is the overcoming of dislocation forests by individual dislocation. The emergence and evolution of a heterogeneous microstructure of dislocations as well as the long-range intersections between dislocations dominates and controls the mechanisms of thermal activation analysis behavior (Armstrong and Zerilli, 1988).

In the modified JC model, the strain rate hardening item $(1 + C(\ln \dot{\varepsilon}_e)^p)$ has two parameters: C and p . The strain rate hardening effect is more significant when both C and p increase together. For martensite or tempered martensite (bcc), the fitting results are: $C = 3.10$, $p = 4.86$. For austenite (fcc), the fitting results are: $C = 2.95$, $p = 4.12$. Both C and p of bcc metal are larger than those of fcc metal. It behaves that bcc metal exhibits higher sensitivity of strain rate compared to fcc metal.

The width of a single-phase block in Fig. 17 is a measurement of sensitivity on strain rate. Each block contains six curves in which the strain rate increase from low to high. Regarding the hardening effect of the strain rate, the higher strain rate curve is on top of the lower strain rate curve. The sensitivity of strain rate is higher when the block is wider. The yellow block (bcc) is wider than the cyan block (fcc). The width of colored block corresponds well with parameters C and p .

The slope of the single-phase block in Fig. 17 is a measurement on the sensitivity of temperature. The yellow block (bcc) has a large slope than the cyan one (fcc). It behaves that the bcc metal has a high sensitivity of temperature than the fcc metal.

6.3. Comparison of the original JC model and modified JC model

The original JC model is an empirical constitutive model for metals subject to large strains, high strain rates and high temperatures. As shown in Eq. (27), the effects of strain, strain rates, and temperature on the plastic flow stress are simply integrated into the model as a multiplication form (Johnson and Cook, 1983).

$$\sigma_i(T, \varepsilon, \dot{\varepsilon}) = (A + B\varepsilon_e^n)(1 + C \ln \dot{\varepsilon}_e^*)^{(1 - (T^*)^m)} \quad (27)$$

For the original JC model, the item $\{\frac{\sigma}{(A+B\varepsilon_e^n)(1-(T^*)^m)} - 1\}$ should be a linear relationship with the item $(\ln \frac{\dot{\varepsilon}}{\dot{\varepsilon}_0})$. In the case of the modified JC model in Eq. (3), these two items can be expressed as: $\frac{\sigma}{(A+B\varepsilon_e^n)(1-(T^*)^m)} - 1 = C(\ln \frac{\dot{\varepsilon}}{\dot{\varepsilon}_0})^p$. As shown in Fig. 18, the fitting result shows that original JC model does not provide good fits for both low and high strain rates. The modified one can well describe the data as shown by the red curve.

6.4. Fitting accuracy of the phase-based constitutive model

Due to the phase transformation kinetics involved, the phase-based model has higher prediction accuracy than the single-value model. Fig. 19 shows the predicted stresses calculated by the phase-based model and the original JC model. The slope of the linear fit is typically used to describe the accuracy of the model. The model is more accurate as this value becomes closer to one.

The slopes of the phase-based model and original JC model are approximately 0.98 and 0.82, respectively. The phase-based model

